Zirconolite in metarodingites of Penninic Mesozoic ophiolites, Central Alps

Autor(en): **Stucki, Andreas / Trommsdorff, Volkmar / Günther, Detlef**

Objekttyp: **Article**

Zeitschrift: **Schweizerische mineralogische und petrographische Mitteilungen = Bulletin suisse de minéralogie et pétrographie**

Band (Jahr): **81 (2001)**

Heft 2

PDF erstellt am: **24.09.2024**

Persistenter Link: https://doi.org/10.5169/seals-61692

SCHWEIZ. MINERAL. PETROGR. MITT. 81, 257–265, 2001

Zirconolite in metarodingites of Penninic Mesozoic ophiolites, Central Alps

by *Andreas Stucki*[1], *Volkmar Trommsdorff*[1] and *Detlef Günther*[2]

Abstract

Zirconolite ($CaTi_2ZrO_7$) occurs in metamorphosed rodingitized Fe-Ti-gabbro dikes in the Southern Steep Belt of the Central Alps. The dikes crosscut metaperidotites all forming remnants of a late Jurassic ophiolite suite that has been metamorphosed to upper amphibolite facies during Alpine orogeny. Zirconolite occurs as fragmented grains and small needles and overgrowths on ilmenite. It is accompanied by clinopyroxene, magnesian ilmenite, spinel, chlorite and pseudomorphs after titanian clinohumite. Locally, zirconolite is corroded and replaced by zircon which contains CO_2-bearing fluid inclusions. Zirconolite shows extensive cation substitution of the type $Ca + Ti \leftrightarrow REE^{3+}Fe^{3+}$, whereby up to 25% of Ti is replaced by Fe^{3+} and up to 50% of Ca by REE and Y. The REE contents are 1 to 5×10^4 times chondritic with the exception of La (0.5×10^4). In addition, baddeleyite occurs in a blackwall nearby. It contains unusually high Si, Al, Mg and Ti. The zirconolite clusters are interpreted as of magmatic origin. The zirconolite overgrowths and the zircon generation enclosing zirconolite are likely of metamorphic origin. P-T conditions of metamorphism are estimated at 0.6–0.7 GPa and 700 to 750 °C.

Keywords: zirconolite, zircon, baddeleyite, Southern Steep Belt, ophiolite, metarodingite.

Introduction

Zirconolite is a rare mineral and so far has been reported from approximately 60 localities, of which 7 are lunar (WILLIAMS and GIERÉ, 1996; GIERÉ et al., 1998). This limited number of reported occurrences may be explained in part by its inconspicuous appearance. It is usually of very small size and strongly resembles other dark-colored accessory minerals like rutile, ilmenite or perovskite. Zirconolite is generally found in silica-poor rocks. Hence, most occurrences of zirconolite are described from silica-undersaturated alkalic magmatites such as carbonatites, kimberlites and syenites. Additionally however, a remarkable variety of host rock types was reported: different sorts of metasomatic rocks, lunar rocks, carbonate and ultramafic rocks and one gabbroic rock (FOWLER and WILLIAMS, 1986). An overview is given by WILLIAMS and GIERÉ (1996).

The composition of zirconolite can deviate significantly from the original stoichiometric formula ($CaTi_2ZrO_7$). Substitutions involve mainly rare earth elements (REE) and yttrium, actinides, hafnium, niobium, tantalum and iron. As actinides can be incorporated in high quantities, zirconolite is of technical interest and is under examination as a promising option for the immobilization of high level nuclear waste (e.g. SYNROC, e.g. LUMPKIN et al., 1991, 1994; MALMSTRÖM et al., 1999).

From a geological point of view, the significant incorporation of REE, Nb, Ta, U and Th could make zirconolite a useful indicator of the bulk trace element budget.

In Switzerland, zirconolite was previously found together with allanite and hoegbomite in a marble skarn of the Bergell contact aureole by GIERÉ (1986). This is the second reported occurrence of zirconolite and the first one for baddeleyite in Switzerland.

[1] Institut für Mineralogie und Petrographie, ETH-Zentrum, CH-8092 Zürich, Switzerland. <andreas.stucki@erdw.ethz.ch>

[2] Laboratorium für Anorganische Chemie, ETH-Zentrum, CH-8092 Zürich, Switzerland.

Analytical methods

Electron microprobe analysis (EMPA): Zirconolites from all three dikes were analyzed using a Cameca SX-50 electron microprobe. Of the REE, La, Ce, Pr, Nd, Sm and Gd were measured and intra-REE spectral interferences, affecting mainly Pr, considered. Other trace elements analyzed include Nb, Ta, Hf, U and Th. Operating parameters include an acceleration potential of 15 kV, a beam current of 20 nA and a beam size of approx. 1 μm. Natural and synthetic elements, oxides and silicates were used as standards. Measuring time for major elements was 20 seconds and for trace elements 30 to 40 seconds.

Laser ablation microprobe-inductively coupled plasma spectrometry (LAM-ICP-MS): A 193 nm excimer laser (Compex 110I, Lambda Physik, Göttingen, Germany) in combination with an ELAN 6000 ICP-Mass Spectrometer (Perkin Elmer, Norwalk, USA) have been used for in situ trace element determinations in zirconolite, zircon and baddeleyite. Due to grain size, only the large zirconolite grains from sample GR15.9 were analyzed by LAM-ICP-MS. Details about the LAM-ICP-Ms system are described by GÜNTHER et al. (1997). Background was acquired for 30 s and approx. 60 s have been used for mineral analysis. Calibration has been carried out using NIST standard 612 as an external standard, and the EMPA-measured contents of Al, Si and/or Ca of the mineral samples have been used as internal standards. Data show excellent agreement between EMPA and LAM-ICP-Ms for non-matrix-matched calibration. The direct comparison of EMPA and LAM-major elements allows the determination of the accuracy and the reproducibility of the results. If the majors are in between 10% for two independent matrices, trace elements should have the same deviation. The limits of detection in a 40 μm pit are approx. 40 ppb (depending on the mass and abundance). Pit sizes in the analyzed Zr-minerals are 10 to 20 μm.

Regional geology

The Zone of Bellinzona-Dascio (ZBD) represents the southernmost Penninic unit of the Central Alps (KNOBLAUCH and REINHARD, 1939). Metamorphic ophiolitic relics consisting of metaperidotites and metarodingites, gneisses, amphibolites and rare carbonate rocks occur in this east–west striking, approximately 50 km long and 5 km wide zone (FUMASOLI, 1974; HEITZMANN, 1975; TROMMSDORFF and EVANS, 1979; HANSMANN, 1980; EVANS et al., 1981, BÜHL, 1980; SCHMIDT, 1989). The largest metaperidotite body within the ZBD, the Gana Rossa, was mapped by KNOBLAUCH (1939), FUMASOLI (1974) and SCHMIDT (1989). It is here where zirconolite has recently been found (Fig. 1).

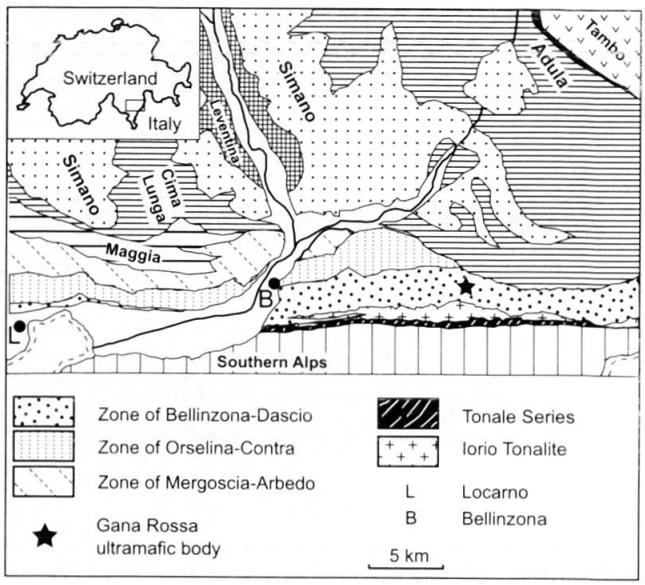

Fig. 1 Tectonic map of the southern Central Alps.

All lithological units of the ZBD are of uppermost amphibolite facies grade. No traces of a previous high-pressure metamorphism have been observed. Conditions of metamorphism are estimated at 700 to 750 °C and 0.6 to 0.7 GPa based on thermobarometry in pelitic and mafic rocks (HEITZMANN, 1975; BÜHL; 1980; SCHMIDT,

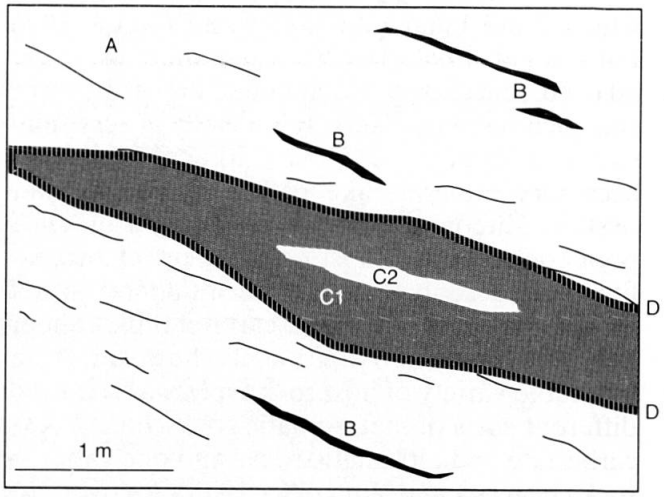

Fig. 2 Schematic sketch of the zirconolite occurrence at Gana Rossa. A = host metaperidotite, B = zirconolite-bearing ilmenite-clinopyroxenite dikelets, C1 = rodingitized former Fe-Ti-gabbro with inclusions of a rodingitized former Mg-gabbro (C2). D = blackwall. Note that a direct connection between dikelets and metarodingite is missing and was probably erased by Alpine deformation.

1989; BUOB, 1997) as well as in ultramafic rocks (STUCKI, 2001).

The metarodingites occur as boudinaged dikes in the metaperidotites. Chemically, they show a large variability and are derived from Mg-gabbros, Fe-Ti-gabbros, basalts or rare oceanic granites ("plagiogranites"). Despite rodingitization, the contents and ratios of diagnostic trace elements (e.g. Ti, Zr, REE) are more or less unaltered and are typical of a tholeiitic differentation trend. This association of mantle rocks, Mg- to Fe-Ti-gabbros, plagiogranites and basalts in the Alps is typical for ophiolites originating from the Jurassic Piemont-Ligurian ocean. U/Pb dating on zircons from two former plagiogranite dikelets near the Gana Rossa yields a late Jurassic age of 148 ± 3 Ma and 141 ± 6 Ma. The geochemistry and age of the Bellinzona ophiolites are discussed in more detail in STUCKI (2001).

The host rock

Zirconolite was found in three small dikes of clinopyroxenite consisting of diopside, magnesian ilmenite, green spinel and chlorite (samples GR3.2, GR15.9 and GR17.2). Minerals that are normally found in rodingitized Fe-Ti-gabbros in the Zone of Bellinzona-Dascio (TROMMSDORFF and EVANS, 1979; SCHMIDT, 1989) such as andradite, titanite and perovskite, are absent.

One of these dikes (GR15.9) contains conspicuous textures of olivine with oriented, wormy Mg-ilmenite inclusions. This olivine is very forsterite-rich (Fo_{95}) and ilmenite is enriched in Mg, with X_{geik} up to 0.45. Such textures are similar to those reported by TROMMSDORFF and EVANS (1980) and interpreted as the breakdown product of OH-titanian clinohumite. The other two dikes (GR17.2 and GR3.2) contain no olivine-ilmenite intergrowths but are otherwise very similar.

The three zirconolite-bearing dikes occur within a few meters distance to a relatively large rodingitized former Fe-Ti-gabbro dike containing inclusions of rodingitized former Mg-gabbro (Fig. 2). Compositionally, it is characterized by a modest REE-enrichment. Its REE pattern exhibits a positive Eu anomaly which is uncommon for the former Fe-Ti-gabbros that normally exhibit a negative Eu anomaly (Fig. 5). The included former Mg-gabbro shows typical low REE abundance with a strong positive Eu anomaly (Fig. 5). As is illustrated in figure 2, a direct connection between the zirconolite-bearing rocks and the large former Fe-Ti-gabbro dike was not observed in the field but may have been obliterated by Alpine deformation.

Baddeleyite was found in a small dike that crops out near the zirconolite-bearing dikes. However, its presence may be unrelated to the occurrence of zirconolite. The baddeleyite-bearing dike now shows a typical blackwall assemblage consisting of olivine, magnesian ilmenite, magnesio-hornblende and chlorite. Abundant zircon and minor apatite also occur.

Zirconolite

APPEARANCE

Zirconolite is free of inclusions and, in thin section, has a uniform brown color. Its appearance differs somewhat from one dikelet to the other:

1. In sample GR15.9, zirconolite appears as large patches of almost millimeter size. These patches seem intensely fractured and may rather be clusters of individual small (10 to 50 μm) subgrains, as revealed in crossed polarized light. Often, the outline of the clusters is very irregular (Fig.3a).
2. In dike GR17.2, zirconolite is found dispersed as small (20 to 50 μm) grains throughout the clinopyroxene-oxide matrix. The grains themselves are similar in appearance to GR15.9 as they also occur as clusters of small individual crystals. The clusters are much smaller in this dike, only reaching diameters of 100 μm in the clinopyroxene matrix.
3. The third zirconolite-bearing dike (GR3.2) is the largest in size. Although the assemblage of the dike is basically the same as that in GR17.2 and GR15.9, zirconolite from this dike is quite different in appearance. It is found as tiny needles and anhedral blades attached to large, cm-sized ilmenite-ulvospinel clusters. Tiny zircon crystals also occur near the ilmenite-ulvospinel clusters. Zirconolite individuals range in size from 10 to 30 μm (Fig. 3b).

CHEMICAL COMPOSITION

EMPA and LAM-ICP-Ms analyses of zirconolite are listed in tables 1 and 2. As is typical for natural zirconolite (see WILLIAMS and GIERÉ, 1996), Ca shows the strongest deviation from stoichiometry. Most grains only contain 8 to 9 wt% CaO, compared with 16.5 wt% CaO in stoichiometric zirconolite. Titanium also displays significant deficiency: 33.7 to 36.3 wt% compared with 47.10 wt% TiO_2. ZrO_2 ranges from 31.45 to 34.84 wt%, being quite close to ideal values (36.34 wt%). Iron is an important constituent, a feature well known from other occurrences (WILLIAMS and GIERÉ,

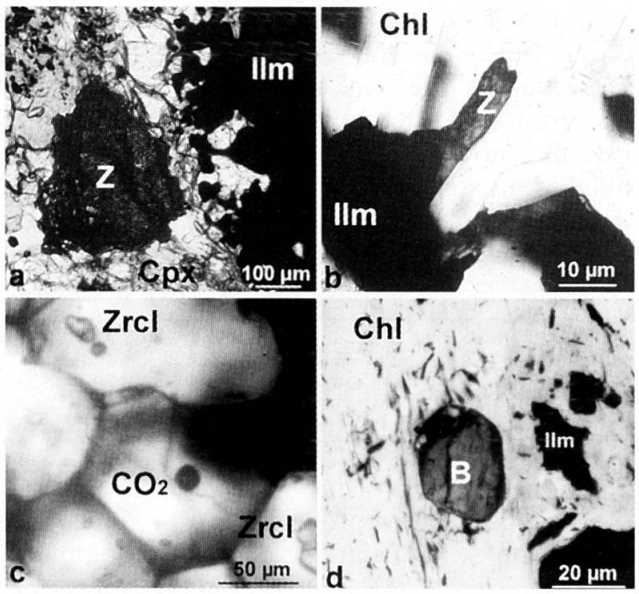

Fig. 3 (a) Zirconolite (Z) cluster (from GR15.9) associated with ilmenite and clinopyroxene. (b) Needle-shaped zirconolite (Z) sitting on ilmenite (GR3.2) in a chlorite-rich groundmass. (c) Zircon grains with inclusions of amoeboid zirconolite (Zrcl) and CO_2-bearing fluid inclusions (CO_2). (d) Baddeleyite (B) crystal with chlorite and ilmenite.

1996), with values ranging from 5 to 8.5 wt% Fe_2O_3. Al_2O_3 is constant at 0.4 to 0.5 wt% in GR15.9 and GR17.2 but is distinctly lower in GR3.2, where it averages 0.3 wt%. Of the elements Si, Mn and Mg, only Mg is above the detection limit: MgO contents vary from 0.08 to 0.25 wt%. The low totals in table 1 may be explained by significant amounts of HREE which were not analyzed by electron microprobe.

RARE EARTH ELEMENTS

In all three dikes, zirconolite is remarkably rich in REE and Y. Yttrium is the most abundant element and may be as high as 7.45 wt% Y_2O_3 in zirconolites from GR17.2. In GR15.9, it varies between 4.95 and 6.90 wt%. It is markedly lower in dike GR3.2 where it ranges from 5.4 down to 3 wt% Y_2O_3. Of the Lanthanides, Ce_2O_3, Nd_2O_3 and Dy_2O_3 show the highest absolute concentrations: maximum percentages in GR15.9 zirconolites measured by LAM-ICP-MS are 1.0 wt%, 1.4 wt% and 1.3 wt%, respectively. Some microprobe analyses in GR17.2 show even higher values: 1.87 wt% Ce_2O_3 and 1.93 wt% Nd_2O_3. Zirconolites from GR3.2 are comparably depleted in REE: Ce_2O_3 is between 0.5 and 0.75 wt%, Nd_2O_3 between 0.5 and 0.87 wt%.

Zirconolite from GR15.9 displays relatively flat CI-chondrite normalized REE patterns with a marked LREE depletion and enrichment up to 5.5×10^4 relative to chondrite values (Fig. 5). Eu shows a positive anomaly with Eu* [= $Eu_N/\{(Sm_N+Gd_N)/2\}$] ranging from 1.23 to 1.39. LREE such as La, Ce and Pr show enrichment below a factor of 2×10^4. Relative enrichments of Gd through Lu are all approximately 3×10^4. Although only zirconolite from GR15.9 was analyzed for all REE, it is probable that zirconolites from the other two dikes show a similar REE pattern.

While the small zirconolite crystals from GR3.2 appear to be homogeneous, a weak zonation was noticed in the zirconolite clusters in GR15.9 and GR17.2, with a slight LREE depletion towards the cluster rims. The zonation occurs irrespective of the subgrain boundaries within the clusters (Fig. 4).

OTHER MINOR ELEMENTS

Niobium and tantalum, known for having high concentrations in several zirconolites, especially in those occurring in carbonatites (WILLIAMS and GIERÉ, 1996), are almost negligible, i.e. < 0.15 wt% Nb_2O_5 and < 0.012 wt% Ta_2O_5. Uranium and Th, often responsible for metamictization of natural zirconolite when present in sufficient amounts and/or in sufficiently old zirconolite (e.g. GIERÉ, 1986; WILLIAMS and GIERÉ, 1988), are minor constituents. UO_2 ranges from 0.02 to 0.19 wt% and ThO_2 from 0.05 to 0.38 wt%, respectively. Hafnium, always present in Zr-bearing minerals, is only of minor importance: HfO_2 contents do not exceed 0.9 wt%. The Zr/Hf ratio is close to chondritic. Other trace elements such as W and Sc show relatively low abundances: W ranges from 140 to 270 ppm, Sc from 300 to 500 ppm.

Zircon overgrowths on zirconolite

Apart from clusters of zirconolite, dike GR15.9 also contains zircon both as individual grains and as rims around some of the large zirconolite clusters. Some of the zircon contains small amoeboid zirconolite inclusions as well as small fluid inclusions (Fig. 3c). Raman microspectroscopy studies reveal the presence of carbon dioxide and water in these inclusions. This contrasts with fluid inclusions commonly observed in the metarodingite minerals (garnet and diopside) that so far proved to be CO_2-free liquid with minor NaCl (GIANETTONI, 1997; STUCKI, 2001). As can be seen in figure 7, zircon rimming zirconolite partially in-

herits the REE pattern of zirconolite, including the positive Eu anomaly as well as the comparably high LREE contents. One large grain of zircon without zirconolite inclusions also shows a distinct positive Ce anomaly, but with lower total REE contents.

Baddeleyite

Baddeleyite occurs as very small (up to 30 μm) euhedral grains (Fig. 3d) in a chlorite–spinel–ilmenite–olivine vein in the Gana Rossa. In this sample, zirconolite is absent, whereas zircon is relatively common occurring as dispersed single

Tab. 1 EMPA analyses of zirconolite from all three occurrences: mean values and standard deviations.

	GR17.2 (n=4)		GR3.2 (n=3)		GR15.9 (n=8)	
wt%	mean	s.dev	mean	s.dev	mean	s.dev
CaO	7.87	0.62	11.04	1.01	8.67	0.30
TiO_2	34.3	0.78	37.2	0.49	35.7	0.57
ZrO_2	32.6	0.28	35.6	0.92	32.5	0.89
Al_2O_3	0.39	0.03	0.30	0.01	0.45	0.02
Fe_2O_3 (total Fe)	7.84	0.91	5.60	1.44	6.96	0.10
MnO	<0.02		<0.02		<0.02	
MgO	0.15	0.08	0.13	0.04	0.16	0.02
Y_2O_3	6.88	0.81	4.53	1.03	6.40	0.38
La_2O_3	0.18	0.12	0.13	0.06	0.18	0.06
Ce_2O_3	1.43	0.19	0.79	0.05	1.33	0.27
Pr_2O_3	0.31	0.04	<0.14		0.28	0.09
Nd_2O_3	1.49	0.13	0.70	0.25	1.47	0.21
Sm_2O_3	0.56	0.02	0.35	0.11	0.75	0.03
Gd_2O_3	1.16	0.07	0.56	0.16	1.07	0.13
HfO_2	0.37	0.01	0.24		0.64	0.08
Nb_2O_5	0.08	0.04	0.06		0.08	0.03
ThO_2	0.15	0.01	0.06	0.01	0.09	0.06
UO_2	0.22	0.05	<0.05		0.14	0.05
Total	95.88		97.11		96.92	
Normalized to 7 oxygens:						
Ca	0.555		0.725		0.580	
Y	0.228		0.135		0.212	
La	0.004		0.003		0.004	
Ce	0.033		0.018		0.030	
Pr	0.007		0.002		0.006	
Nd	0.034		0.016		0.032	
Sm	0.013		0.008		0.016	
Gd	0.024		0.012		0.022	
Th	0.002		0.001		0.001	
U	0.004		0.001		0.002	
Total Ca	0.901		0.917		0.904	
Ti	1.637		1.722		1.676	
Al	0.030		0.022		0.033	
Fe	0.370		0.259		0.326	
Mn	0.000		0.000		0.000	
Mg	0.014		0.012		0.015	
Nb	0.002		0.002		0.002	
Total Ti	2.052		2.016		2.052	
Zr	1.010		1.049		0.990	
Hf	0.007		0.003		0.011	
Total Zr	1.016		1.053		1.002	
Sum Cations	3.969		3.986		3.957	
O	7		7		7	

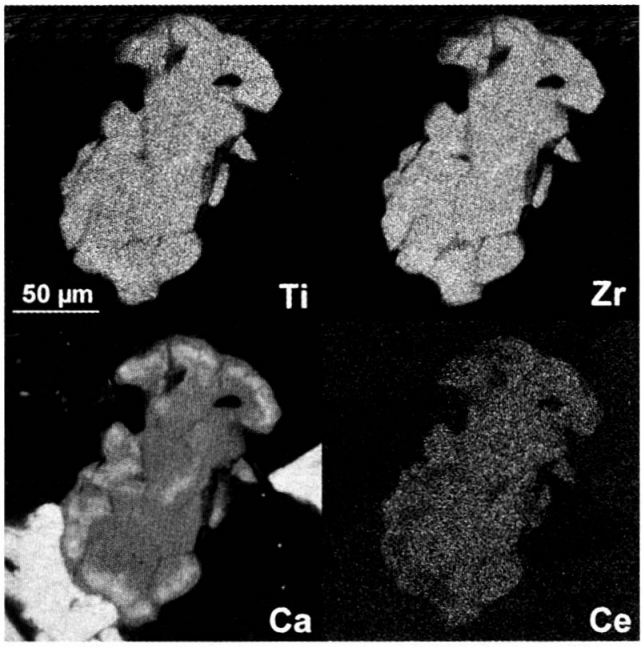

Fig. 4 Element distribution images of a small zirconolite grain cluster in GR17.2. Internal grain boundaries are well visible in the Ca-image. Bright areas are rich, dark areas poor in the respective element.

Tab. 2 LAM-ICP-MS analyses of zirconolite from GR15.9.

wt%	1	2	3	4
Al_2O_3	0.87	0.62	0.67	0.71
TiO_2	37	37	38	37
Sc_2O_3	0.074	0.057	0.081	0.077
V_2O_5	0.063	0.085	0.085	0.065
Y_2O_3	5.58	4.90	6.91	5.56
Nb_2O_5	0.12	0.11	0.14	0.15
La_2O_3	0.06	0.10	0.07	0.07
Ce_2O_3	0.68	1.01	0.83	0.79
Pr_2O_3	0.15	0.20	0.18	0.16
Nd_2O_3	1.19	1.32	1.38	1.25
Sm_2O_3	0.62	0.55	0.69	0.63
Eu_2O_3	0.33	0.27	0.37	0.30
Gd_2O_3	0.85	0.69	0.96	0.88
Tb_2O_3	0.15	0.13	0.19	0.17
Dy_2O_3	1.08	0.90	1.29	1.21
Ho_2O_3	0.22	0.20	0.29	0.27
Er_2O_3	0.63	0.60	0.84	0.79
Tm_2O_3	0.09	0.09	0.12	0.11
Yb_2O_3	0.50	0.55	0.71	0.65
Lu_2O_3	0.06	0.08	0.09	0.09
Ta_2O_5	0.01	0.01	0.01	0.01
WO_3	0.02	0.02	0.04	0.03
ThO_2	0.12	0.10	0.13	0.19
UO_2	0.17	0.19	0.30	0.38
$SREE_2O_3$ $+Y_2O_3$	12.18	11.59	14.90	12.92
(ppm)				
Zn	2.9	37.6	36.4	56.7
Sr	2.3	3.6	6.5	7.3
Pb	12.9	7.3	7.7	14.7
Bi	12.9	13.9	12.0	11.5

grains. Compositionally, baddeleyite is remarkably impure (see table 3): Only 75 wt% are ZrO_2. On the other hand, it has high contents of SiO_2 (4 to 5.5 wt%), TiO_2 (approx. 3.5 wt%), Al_2O_3 (5.5 to 7.5 wt%) and, most surprisingly, large amounts of MgO (6 to 7.9 wt%). However, BSE and element distribution imaging reveals baddeleyite to appear homogeneous and free of inclusions.

REE contents in baddeleyite are below the detection limits of the EMPA, but these elements have been determined by LAM-ICP-MS. Baddeleyite shows smooth HREE enrichment up to 1300 times chondritic values (Fig. 7). Thorium and U concentrations are low, 6 ppm and 32 ppm, respectively; Sc and V are slightly enriched with 0.11% Sc_2O_3 and 0.09% V_2O_5. However, because of its scarcity and small grain size, only one grain was analyzed in detail and the results are tentative.

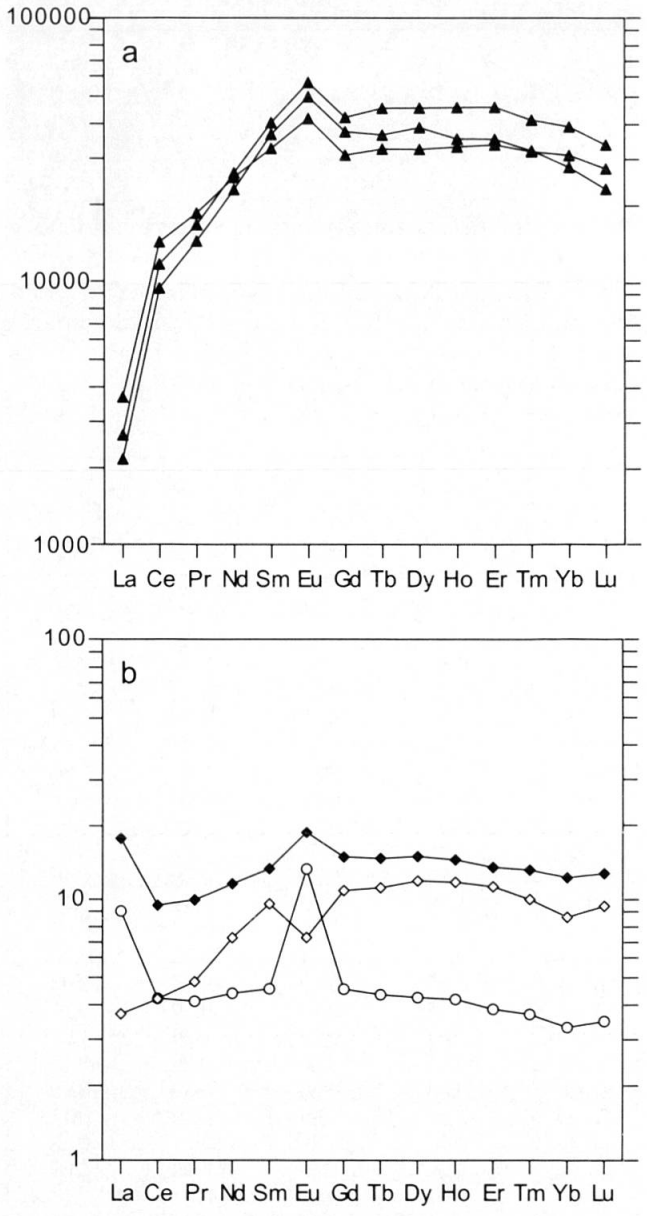

Fig. 5 (a) CI-Chondrite-normalized REE patterns of zirconolite from GR15.9. Normalization values by SUN and MCDONOUGH (1989). (b) CI-chondrite-normalized REE patterns of associated rodingitized former gabbroic rocks. ○ = former Mg-gabbro; ◆ = former Fe-Ti-gabbro dike adjacent to zirconolite-bearing dikes that contains inclusions of a former Mg-gabbro; ◇ = typical former Fe-Ti-gabbro.

Discussion

ZIRCONOLITE COMPOSITION AND SUBSTITUTION MECHANISMS

Iron and REE represent the only significant additional constituents in zirconolite and they correlate positively with each other (Fig. 6). For charge balance reasons, iron consequently is mostly ferric. The coupled substitution $CaTi \leftrightarrow REE^{3+}Fe^{3+}$ thus most probably accommodates most of the REE including Y. They may occupy up to 50% (equivalent to 15 wt% REE_2O_3) of the Ca-site and iron replaces up to 25% of the Ti-site. Possibly, a minor proportion of the HREE may also occupy the Zr-site, although the EMPA analyses suggest that the Zr-site is fully occupied (Tabs 1, 2).

Niobium and Ta are incorporated into the Ti-site, while U and Th may be on either Ca-site or Zr-site (see listing of hypothetical end-members by GIERÉ et al., 1998). These elements, apart from some minor HREE incorporation on the Zr-site and missing HREE EMP analysis, may be responsible that all analyses plot below the line representing the $FeREECa_{-1}Ti_{-1}$-substitution in Fig. 6.

ZIRCONOLITE FORMATION

Zirconolite occurs mostly as fractured clusters of subgrains. The subgrains in the outer parts are slightly poorer in LREE (Fig. 4) and tentatively suggest that these clusters represent formerly single, zoned crystals that recrystallized to subgrains. According to GIERÉ et al. (1998), the chemical composition of zirconolite reflects the general chemical characteristics and the paragenesis of the host rock. Markedly low Nb, Ta, U, and Th but high REE and Fe concentrations are in fact typical for evolved tholeiitic melts. Additionally, besides La, which cannot be easily accommodated in the zirconolite structure (GIERÉ et al., 1998), the shape of REE patterns of zirconolite indeed resembles that of the adjoining former Fe-Ti-gabbro (regarded as the origin of the ilmenite-clinopyroxene dikelets). Both zirconolite and former Fe-Ti-gabbro show a relative LREE de-

pletion and a noncharacteristic positive Eu anomaly. This anomaly may be explained by interaction of the former Fe-Ti-gabbro melt with the former (Eu-enriched) Mg-gabbro inclusions.

The only other known zirconolites from a gabbroic rock (St. Kilda, FOWLER and WILLIAMS, 1986) are characterized by a REE pattern of similar overall shape (the Eu anomaly however being negative). In fact, of all the known terrestrial occurrences (WILLIAMS and GIERÉ, 1996), the St. Kilda zirconolite composition most closely resembles that of the Gana Rossa zirconolites with respect to overall REE, Nb, Ta, U and Th contents. Consequently, with the exception of the small single crystals from GR3.2, it is likely that zirconolite may be a remnant igneous mineral, incorporating much of the available bulk REE (including a positive Eu anomaly). In-situ subgrain formation that produced the clusters then occurred most likely during Alpine deformation and metamorphism.

Tab. 3 EMPA and LAM-ICP-MS analyses of zircon associated with zirconolite in GR15.9 and baddeleyite in GR17.1. LAM-ICP-MS analyses are standardized to 32% SiO_2 (zircon) or 5.5% SiO_2 (baddeleyite).

EMPA	Zircon		Baddeleyite	
wt%	GR15.9 (n=3)	s.dev	GR17.1 (n=3)	s.dev
MgO	<0.02		7.01	0.69
Al_2O_3	<0.03		6.62	0.82
SiO_2	32.10	0.14	5.59	0.04
CaO	0.06	0.06	0.37	0.02
TiO_2	<0.02		3.47	0.11
MnO	<0.02		0.03	0.02
Fe_2O_3	0.19	0.03	1.97	0.28
Y_2O_3	0.09	0.02	0.09	0.04
ZrO_2	65.29	0.66	73.97	1.34
HfO_2	1.24	0.22	1.59	0.21
ThO_2	<0.05		<0.05	
UO_2	<0.05		<0.05	
P_2O_5	0.04	0.01		
Total:	98.99		100.68	

LAM-ICP-MS	Zircon[1]	Zircon[2]	Baddeleyite
Al_2O_3 (wt%)	0.06	0	6.72
TiO_2 (wt%)	0.55	0	3.55
Sc (ppm)	355.6	325.0	713.2
V	12.71	8.05	503.85
Zn	5.92	0.1	29.06
Y	1155	292.4	654.0
Nb	13.27	0.02	137.5
La	9.77	0.02	19.93
Ce	98.39	11.55	76.9
Pr	20.16	0.22	15.61
Nd	155.5	1.75	78.01
Sm	79.31	0.96	33.79
Eu	40.62	0.92	12.26
Gd	122.2	5.14	42.54
Tb	27.1	1.18	8.52
Dy	209.0	14.72	84.44
Ho	54.83	6.5	22.06
Er	215.8	35.16	113.2
Tm	37.57	9.97	25.84
Yb	296.6	108.3	290.8
Lu	57.31	23.43	50.64
Ta	0.81	0.05	0.68
W	2.52	<0.10	81.48
Pb	0.93	0.13	1.64
Th	37.08	10.21	5.95
U	38.25	8.80	32.67

[1] overgrowing zirconolite.
[2] single grain without zirconolite inclusions.

However, metasomatic formation of zirconolite during serpentinization and concomitant rodingitization of the former gabbros cannot be ruled out. Fluid inclusion studies show that this metasomatic episode mainly involved a relatively pure aqueous fluid with possible minor NaCl (GIANETTONI, 1997; STUCKI, 2001). In such fluids, mobility of the generally incompatible Zr, REE and Ti is expected to be limited and zirconolite is expected to be very durable, even at temperatures in excess of 500 °C (MALMSTRÖM, 2001). This finding is confirmed by the preserved igneous Ti, Zr and REE contents of all metarodingites in the Zone of Bellinzona-Dascio ophiolites (STUCKI, 2001).

Whilst an igneous origin of zirconolite in the dikes GR15.9 and GR17.2 seems probable, the small needles and blades of zirconolite in GR3.2 may have had a different origin. It is possible that the latter zirconolite formed during Alpine metamorphism through a reaction involving ilmenite and associated zircon, for example: $2FeTiO_3 + ZrSiO_4 + CaMgSi_2O_6 \rightarrow CaTi_2ZrO_7 + 3SiO_2 + MgO + 2FeO$, which may also form chlorite if clinopyroxene was Al-bearing. However, this zirconolite may also have formed directly from ilmenite through expulsion of Zr from igneous ilmenite during high-grade metamorphism (cf. BINGEN et al., 2001).

Given that these conclusions are correct, zirconolite from GR15.9 and GR17.2 would have persisted throughout the entire Alpine metamorphic cycle that reached approx. 700 °C at 0.6 to 0.7 GPa.

ZIRCON OVERGROWING ZIRCONOLITE

Zircon, occurring as overgrowths on zirconolite, was formed by hydrothermal activity under the influence of CO_2-and SiO_2-bearing fluids. Experimental work at 550 °C and 50 MPa shows that CO_2- and SiO_2-bearing fluids alone do not facilitate zirconolite corrosion but require additional ions as ligands for the zirconolite constituents (MALMSTRÖM, 2001). In this case, the presence of silica initiated zircon to form instead of baddeleyite. The fate of Ti, Ca and much of the REE is not known (perovskite and titanite are absent). The temperature and pressure conditions of this secondary zircon are unknown.

BADDELEYITE

Baddeleyite, found in one sample nearby as minute grains, either has a very unusual crystal chemistry not yet observed in other occurrences or contains submicroscopic impurities. No conclusions can yet be drawn from these results. Baddeleyite may represent a magmatic relic in a differentiated magmatic (Fe-Ti-gabbroic?) dike that was in turn overgrown by the Alpine blackwall assemblage. It may also have formed during metamorphism through the reaction of zircon and Mg-ilmenite in the absence of Ca. However, obvious reaction textures as they are known from kimberlites (RABER and HAGGERTY, 1979) are missing.

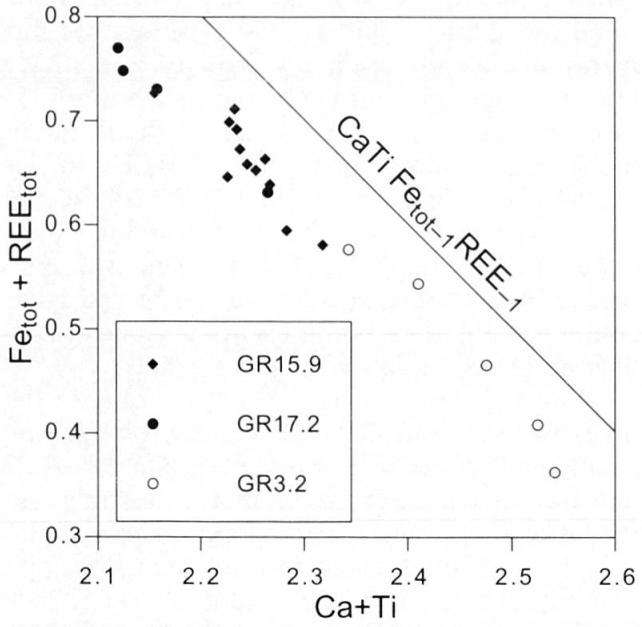

Fig. 6 Correlation between Ca + Ti and Fe_{tot} + REE in zirconolite from all three occurrences. REE include Y.

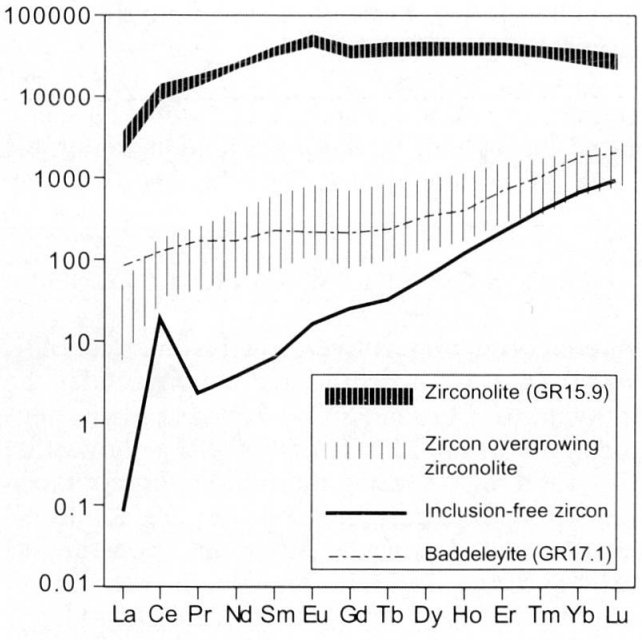

Fig. 7 REE patterns normalized to a CI chondrite (SUN and MCDONOUGH, 1989) of the zirconium bearing phases, measured by LAM-ICP-MS.

FORMER TITANIAN CLINOHUMITE

In addition to zirconolite, olivine-ilmenite intergrowths occur in one of the zirconolite bearing dikelets. Such intergrowths are clearly the product of the breakdown of titanian clinohumite. As is to be expected from the breakdown of OH-titanian clinohumite (TROMMSDORFF and EVANS, 1980), the olivine is very Fo-rich and ilmenite highly magnesian. At a pressure of 0.6 to 0.7 GPa, fluorine-free titanian clinohumite is stable up to temperatures of approx. 600 °C (ENGI and LINDSLEY, 1980). Such temperatures were clearly exceeded in the Zone of Bellinzona-Dascio during the Oligocene metamorphism. Neither titanian clinohumite nor its replacement textures were found in any of the other metarodingites or blackwalls in the ZBD ophiolites.

Conclusions

Zirconolite, occurring in small ilmenite-rich clinopyroxenite dikelets is enriched in REE + Y and Fe which substitute for Ca and Ti, respectively. Due to its appearance as clusters of small individual grains, most of the zirconolite formation seems to predate Alpine metamorphism. An igneous crystallization is suggested by its crystal chemical composition that indicates formation within a highly differentiated tholeiitic melt with low Nb, Ta, U and Th but high REE contents. This suggestion is corroborated by the REE pattern of zirconolite which strongly resembles that of the adjoining former Fe-Ti-gabbro. In-situ recrystallization, preserving some of the zonation of the large crystals, presumably occurred during Alpine dynamic metamorphism.

Locally, zircon replaces zirconolite under the influence of CO_2-bearing fluids. These observations indicate that zirconolite may remain stable up to very high temperatures and moderately high pressures as long as the fluids do not contain CO_2.

Acknowledgments

Support of the Swiss National Science Foundation (Grant 2000-056867.99/1 to V. T.) is gratefully acknowledged. This paper has benefitted from discussions with

R. Gieré and G.R. Lumpkin. Help with electron microprobe REE measurements was kindly provided by E. Reusser. Thorough reviews by R. Gieré and C.T. Williams improved the manuscript substantially.

References

BINGEN, B., AUSTRHEIM, H. and WHITEHOUSE, M. (2001): Ilmenite as a source of zirconium during high-grade metamorphism? Textural evidence from the Caledonides of Western Norway and implications for zircon geochronology. J. Petrol. 42, 335–375.

BÜHL, H. (1980): Petrographie, Metamorphose und Strukturen in der Zone von Bellinzona im Gebiet des Corno di Gesero (GR/TI). Unpublished diploma thesis, ETH Zürich.

BUOB, A. (1997): Considerazioni petrografiche e strutturali dalla regione del Corno di Gesero (TI/GR). Unpublished diploma thesis, ETH Zürich.

ENGI, M. and LINDSLEY, D.B. (1980): The stability of titanian clinohumite: Experiments and thermodynamic analysis. Contrib. Mineral. Petrol. 72, 415–424.

EVANS, B.W., TROMMSDORFF, V. and GOLES, G.G. (1981): Geochemistry of high-grade eclogites and metarodingites from the Central Alps. Contrib. Mineral. Petrol. 76, 301–311.

FOWLER, M.B. and WILLIAMS, C.T. (1986): Zirconolite from the Glen Dessary syenite: a comparison with other Scottish zirconolites. Mineral. Mag. 50, 326–328.

FUMASOLI, M.W. (1974): Geologie des Gebietes nördlich und südlich der Iorio-Tonale-Linie im Westen von Gravedona (Como, It.). Diss. Universität Zürich, 230 pp.

GIANETTONI, T. (1997): Considerazioni petrografiche e strutturali della regione del Corno di Gesero (TI/GR). Unpublished diploma thesis, ETH Zürich.

GIERÉ, R. (1986): Zirconolite, allanite and hoegbomite in a marble skarn from the Bergell contact aureole: implications for mobility of Ti, Zr and REE. Contrib. Mineral. Petrol. 93, 459–470.

GIERÉ, R., WILLIAMS, C.T. and LUMPKIN, G.R. (1998): Chemical characteristics of natural zirconolite. Schweiz. Mineral. Petrogr. Mitt. 78, 435–461.

GÜNTHER, D., FRISCHKNECHT, R., HEINRICH, C.A. and KAHLERT, H.-J. (1997): Capabilities of an Argon Fluoride 193 nm Excimer laser for laser ablation inductively coupled plasma mass spectrometry microanalysis of geologic materials. J. Anal. At. Spectrom. 12, 939–944.

HANSMANN, W. (1980): Geologisch-petrographische Untersuchungen im südlichen Bergell, 2. Val Ligoncio. Unpublished diploma thesis, ETH Zürich.

HEITZMANN, P. (1975): Zur Metamorphose und Tektonik im südöstlichen Teil der Lepontinischen Alpen (Provincia di Como, Italia). Schweiz. Mineral. Petrogr. Mitt. 55, 467–522.

KNOBLAUCH, P. (1939): Blatt Nr. 516, Iorio, 1:25'000; Geol. Atlas der Schweiz. Schweiz. Geol. Komm.

KNOBLAUCH, P. and REINHARD, M. (1939): Erläuterungen zur geologischen Karte, Blatt Nr. 516, Iorio. Kommissionsverlag A. Francke AG, Bern.

LUMPKIN, G.R., SMITH, K.L. and BLACKFORD, M.G. (1991): Electron microscope study of Synroc before and after exposure to aqueous solutions. J. Mater. Res. 6 (10), 2218–2233.

LUMPKIN, G.R., HART, K.P., MCGLINN, P.J., PAYNE, T.E., GIERÉ, R. and WILLIAMS, C.T. (1994): Retention of actinides in natural pyrochlores and zirconolites. Radiochimica Acta 66/67, 469–474.

MALMSTRÖM, J.C. (2000): Zirconolite: Experiments on the stability in hydrothermal fluids. Schweiz. Geotechn. Kommission, Geotechnische Serie Nr. 93, 130 pp.

MALMSTRÖM, J.C., REUSSER, E., GIERÉ, R., LUMPKIN, G.R., DUEGGELIN, M., MATHYS, D. and GUGGENHEIM, R. (1999): Zirconolite corrosion in dilute acidic and basic fluids at 180–700 °C and 50 MPa. In: WRONKIEWICZ, D.J. and LEE, J.H (eds): Scientific Basis for Nuclear Waste Management XXII. Materials Research Society, Boston, USA, 165–172.

RABER, E. and HAGGERTY, S.E. (1979): Zircon-oxide reactions in diamond bearing kimberlites. In: BOYD, F.R. and MEYER, H.O.A. (eds): Kimberlites, Diatremes and Diamonds: Their Geology, Petrology and Geochemistry. Am. Geophys. Union, Washington, D.C., 229–240.

SCHMIDT, M.W. (1989): Petrography and structural evolution of ophiolitic remnants in the Bellinzona Zone, Southern Steep Belt, Central Alps (CH/I). Schweiz. Mineral. Petrogr. Mitt. 69, 393–405.

STUCKI, A. (2001): High-grade Mesozoic ophiolites of the Southern Steep Belt, Central Alps. Unpubl. Ph.D. thesis No. 14206, ETH Zürich.

SUN, S. and MCDONOUGH, W.F. (1989): Chemical and isotopic systematics of oceanic basalts: implications for mantle composition and processes. In: SAUNDERS, A.D. and NORRY, M.J. (eds): Magmatism in the Ocean Basins. Geol. Soc. London Spec. Publ. 42, 313–345.

TROMMSDORFF, V. and EVANS, B.W. (1979): Excursion to Alpe Albion (East of Bellinzona). Excursion of symposium on tectonic inclusions and associated rocks in serpentinites, Genève, Sept. 1979 (unpublished).

TROMMSDORFF, V. and EVANS, B.W. (1980): Titanian hydroxyl-clinohumite: Formation and breakdown in antigorite rocks (Malenco, Italy). Contrib. Mineral. Petrol. 72, 229–242.

WILLIAMS, C.T. and GIERÉ, R. (1988): Metasomatic zonation of REE in zirconolite in a marble skarn at the Bergell contact aureole (Switzerland/Italy). Schweiz. Mineral. Petrogr. Mitt. 68, 133–140.

WILLIAMS, C.T. and GIERÉ, R. (1996): Zirconolite: a review of localities worldwide, and a compilation of its chemical compositions. Bull. Nat. Hist. Mus. London (Geol.) 52(1), 1–24.

Manuscript received January 8, 2001; revision accepted July 13, 2001.